

Coseismic Deformation Time History Calculated from Acceleration Records Using an EMD-Derived Baseline Correction Scheme: A New Approach Validated for the 2011 Tohoku Earthquake

by Jyun-Yan Huang, Kuo-Liang Wen,^{*} Xiao-Jun Li, Jun-Ju Xie, Chun-Te Chen, and Sheng-Chung Su[†]

Abstract Displacement time histories from double-integrated accelerograms typically cannot be used to recover near-field terms because of noise in the acceleration traces. To minimize this problem, empirical mode decomposition (EMD) is used to derive a baseline correction scheme. The scheme is tested against several models composed of a single frequency or two frequencies and offsets in acceleration. It is verified against real displacement time history using Global Positioning Systems (GPS) measurement. For single- and double-frequency-content models, obvious discontinuities are found at drift times for lower intrinsic mode function (IMF) components. A drift model, however, can be clearly found from summing higher IMFs and the residuals of simple frequency-content waveform models. On the other hand, results show that the lesser frequency-content signal has the greater decomposed result. Therefore, a suitable corner frequency for low-pass filtering is first implemented to reduce frequency content. In this case, the trend in the given drift model is easily found by summing higher IMFs for a complex frequency content model (model 3 of this study). A suitable corner frequency for low-pass filtering is attained using a grid-search method. A new semiautomatic EMD-derived baseline correction scheme is tested. The corrected coseismic deformation value (CDV, denoted hereafter as from preevent displacement to the final offset during strong motion), peak ground displacement, and displacement time history from this method have good agreement with 1-Hz continuous GPS measurement for the 2011 Tohoku earthquake.

Introduction

Dense seismic monitoring systems with digital collection systems are now common place across dozens of countries. Additionally, digital data reduce background noise levels, record pre-event histories and first motion data, and provide a wider and more dynamic range (i.e., seismograph with 24 bit or higher) (Boore and Bommer, 2005). Regardless of the greater efficiency and convenience digital data have afforded, problems with determining strong motion close to the source of an earthquake remain. The problem with determining velocity and displacement relates to a phenomenon known as baseline drift (Graizer, 1979; Iwan *et al.*, 1985), which may have its source in ground rotation and tilting at measuring stations (Graizer, 2005, 2006) or in the analog-to-digital conversion process (Boore, 2003; Wang *et al.*, 2003).

Iwan *et al.* (1985) describe the problem of magnetic hysteresis, which occurs during strong ground shaking, and the occurrence of baseline drift. Figure 1 shows the effects of baseline drift as a step function in acceleration data. This results in seriously oblique baselines for the integrals of velocity and displacement. This steplike long-period drift function can be corrected using (1) Fourier-based high-pass filtering to eliminate long-period anomaly (Wang *et al.*, 2003, suggested 0.015-Hz low-cut filtering for the 1999 Chi-Chi, Taiwan, earthquake) or (2) the slope of velocity lines for each part of the acceleration function if suitable time divisions (t_1 and t_2 in Graizer, 1979; Iwan *et al.*, 1985) can be obtained. The problem with (1) is that Fourier-based high-pass filtering results in information loss on permanent displacement. On the other hand, (2) can be difficult because it is not easy to find suitable time divisions. For example, in the case of Taiwan's 1999 Chi-Chi earthquake, Boore (2001) realized that unsuitable time divisions could lead to great divergence in near-fault strong motion. Boore *et al.*

^{*}Also at National Center for Research on Earthquake Engineering, Taipei 10668, Taiwan (R.O.C.).

[†]Also at Central Weather Bureau, Taipei 10048, Taiwan (R.O.C.).

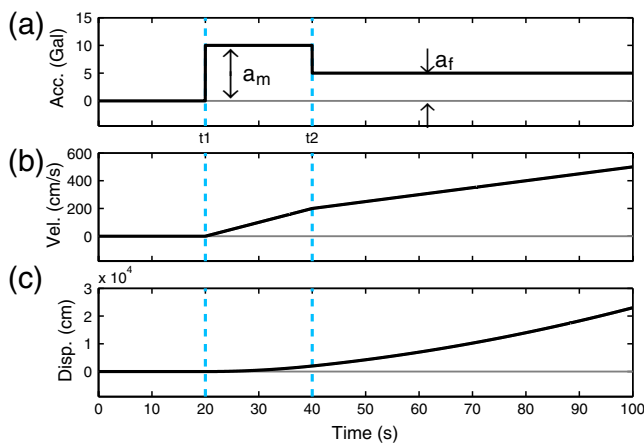


Figure 1. Three-part baseline drift model in (a) acceleration, (b) velocity, and (c) displacement time history. t_1 and t_2 time represent time divisions; a_m and a_f mean drift offset values for each part. (Based on Iwan *et al.* [1985]). The color version of this figure is available only in the electronic edition.

(2002) used a quadratic fitting technique to 1999 Chi-Chi earthquake velocity data to correct the record of Boore (2001) but still produced variance in the permanent displacement record.

Wu and Wu (2007) added an important time parameter t_3 to calculations to help recover some of the lost coseismic displacement; t_3 is the point in time at which displacement time history becomes a straight flat line. They calculated the determined parameter to find the optimal correction result from a grid-search scheme for different divisions of time pairs. In order to reduce manual decision making in the above grid-search scheme, Chao *et al.* (2010) minimized misfit between observation and calculation in a study of the 2003 Chengkung, Taiwan, earthquake. They assumed t_1 and t_3 could be automatically chosen from the accumulated energy of uncorrected acceleration. Wang *et al.* (2011) improved the above approach by following a scheme in which baseline correction is determined by the long-time behavior of corrected displacement seismograms. The improved automatic baseline correction scheme is also based on a step-function fitting process such that the real displacement history after correction fits the step function. This relates to a quite short rise time due to the rupture process being temporally short at the fault.

On the other hand, rotation and tilting motion are the important issues within the fact of baseline drift; they are usually considered as a part of drift noise and were negligible from many researches. Graizer (2005) considered the equations of pendulum behavior and identified tilt effects using numerical experiments. Graizer (2006) constructed an algorithm to extract tilt information from free field and building response during earthquakes. The contributions of tilt involved in drift noise can be measured if the six-component seismograph (three translational and three rotational) can be applied more widely.

As mentioned, the steplike long-period drift function assumed by Graizer (1979) and Iwan *et al.* (1985) can be corrected using Fourier-based high-pass filtering for the elimination of long-period anomalies; however, this results in a permanent loss or contortion of displacement information. There are two different signal analysis techniques that can be applied to this problem. They are (1) discrete wavelet transform (DWT) and (2) empirical mode decomposition (EMD). DWT is a quadrature mirror filter technique that splits an input signal into two bands, allowing for several different frequency-content modes (Mallat, 1989). The EMD method is a relatively new signal analysis method that allows complicated datasets to be decomposed into a finite number of components known as intrinsic mode functions (IMFs). EMD is useful for nonstationary and nonsinusoidal signal decomposition (Huang *et al.*, 1998). This is the main method used in this study. Each IMF decomposed from EMD can be described characteristically as “the higher the decomposed mode, the lower the frequency content” (Zhang *et al.*, 2003). The EMD process can be interpreted as a filter bank of overlapping band-pass filters for the case of fractional Gaussian noise (Flandrin *et al.*, 2004).

The EMD method was first applied to deal with baseline correction problems from strong-motion data of the 1999 Chi-Chi, Taiwan, earthquake. The baseline drift problem for velocity (Fig. 1b) was treated as a final residual in the EMD process owing to the final residual needing to be a monotonic function from which no more IMF can be extracted (Huang *et al.*, 1998). The value of coseismic deformation after eliminating the residual for velocity, however, showed some disagreement with Global Positioning Systems (GPS) data at station TCU129 (Huang *et al.*, 2001). Additionally, a three-phase DWT-based baseline correction scheme that combined decomposition results from acceleration and velocity together to get suitable value for permanent displacement was made for near-fault strong-motion records of the same earthquake (Chen and Loh, 2007). Decomposed lower frequencies subband from discrete Fourier transform construct a reasonable drift model for station TCU068 during the 1999 Chi-Chi, Taiwan, earthquake. Translational in three components and rotational motion in horizontal components are identified (Chanerley and Alexander, 2010). Recently, an improved EMD procedure has been released that makes each IMF more stable, reasonable, and available in nonsinusoidal signal decomposition (Wu and Huang, 2008). This might provide an opportunity to solve baseline drift from decomposing the steplike drift model for acceleration but not the velocity residual. In this study, the improved EMD process for acceleration data is used to verify its ability to correct baseline drift problems. Corrected displacement agrees well with GPS data in many cases.

Empirical Mode Decomposition Method

The Hilbert–Huang transform consists of two parts: the EMD method and the instantaneous frequency of Hilbert

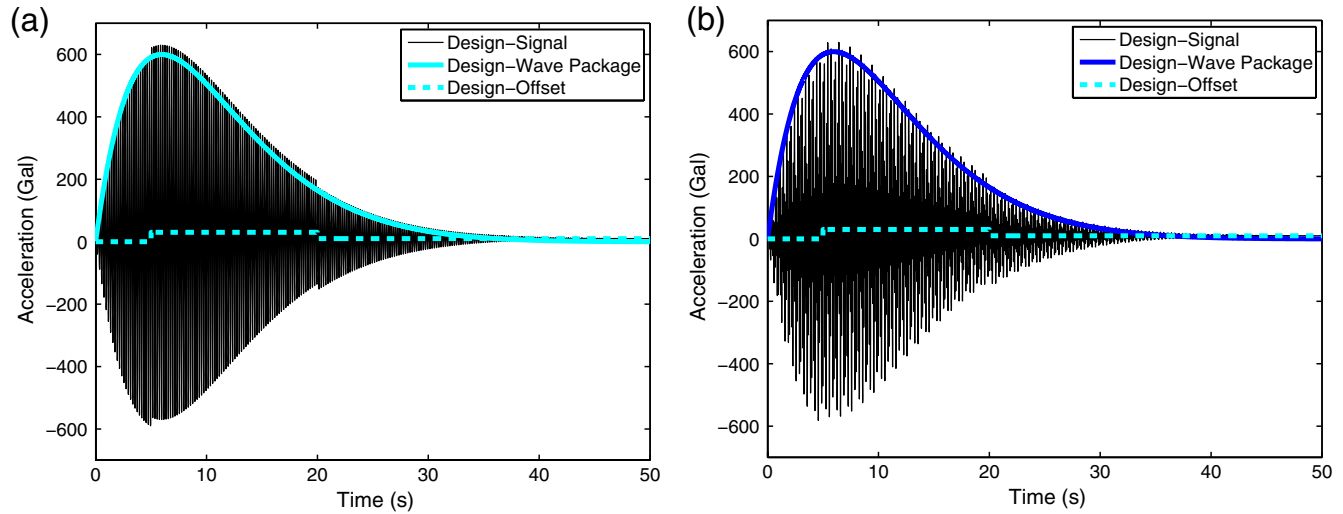


Figure 2. Numerical waveform models with obvious offset. (a) Single-frequency content (model 1): offset is at 5 (30 Gal) and 20 (10 Gal) s. (b) Double-frequency content (model 2): the offset is at 5 (30 Gal) and 20 (10 Gal) s. The color version of this figure is available only in the electronic edition.

spectral analysis. The well-behaved Hilbert transforms need the IMF components to describe frequency content of data in full. The EMD method decomposes a digital signal into several IMFs (Huang *et al.*, 1998). For a complex signal $X(t)$, the sifting process for EMD is as follows:

$$X(t) - m_1 = h_1, \quad (1)$$

where m_1 is the mean of upper and lower envelope lines deduced from local maximum and local minimum values for the whole of the data, and h_1 is the difference between data $X(t)$ and m_1 . The sifting process has two purposes: (1) to eliminate riding waves, make whole trace became a monotonic function; and (2) to make wave profiles more symmetric. Toward this end, the sifting process has to be repeated many times. In the second sifting process, h_1 is treated as the second dataset and so on:

$$h_1 - m_{11} = h_{11}. \quad (2)$$

Repeating these calculations k times is shown as

$$h_{1(k-1)} - m_{1k} = h_{1k}. \quad (3)$$

The sifting processes ends when most of the local maximums are positive and local minimums are negative; at this point h_{1k} becomes IMF c_1 ; that is,

$$c_1 = h_{1k}. \quad (4)$$

In order to determine how many times the sifting process needs to be performed to derive one IMF, Wu and Huang (2008) calculated the sifting number for the IMFs of two similar signals (i.e., signals of no more than 10% difference). The results showed IMFs between the two signals were stable

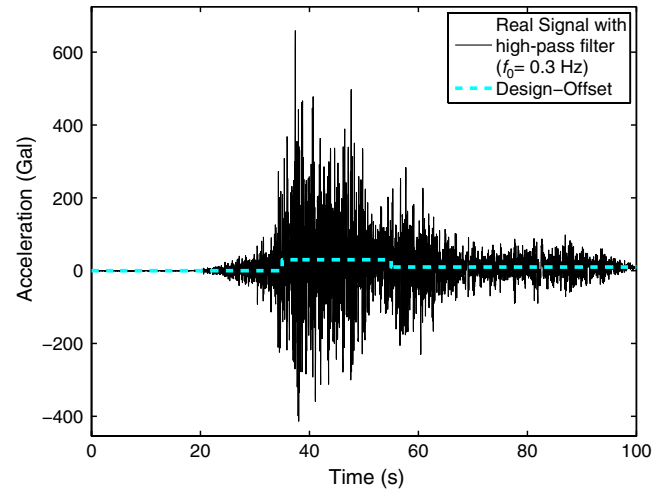


Figure 3. The numerical waveform model made from Z component of station 51SFB for the May 2008 Wenchuan, China, earthquake with high-pass filtering (corner frequency $f_0 = 0.3$ Hz) first and added obvious offset at 35 (30 Gal) and 55 (10 Gal) s (model 3). The color version of this figure is available only in the electronic edition.

when k was fixed at 10. This paper also follows a procedure of $k = 10$ for each IMF c .

After one IMF c_1 is decomposed, the residual is the original data minus c_1 :

$$X(t) - c_1 = r_1. \quad (5)$$

Because the residual r_1 still contains information of longer period components, it was treated as new data and the procedure repeated such that

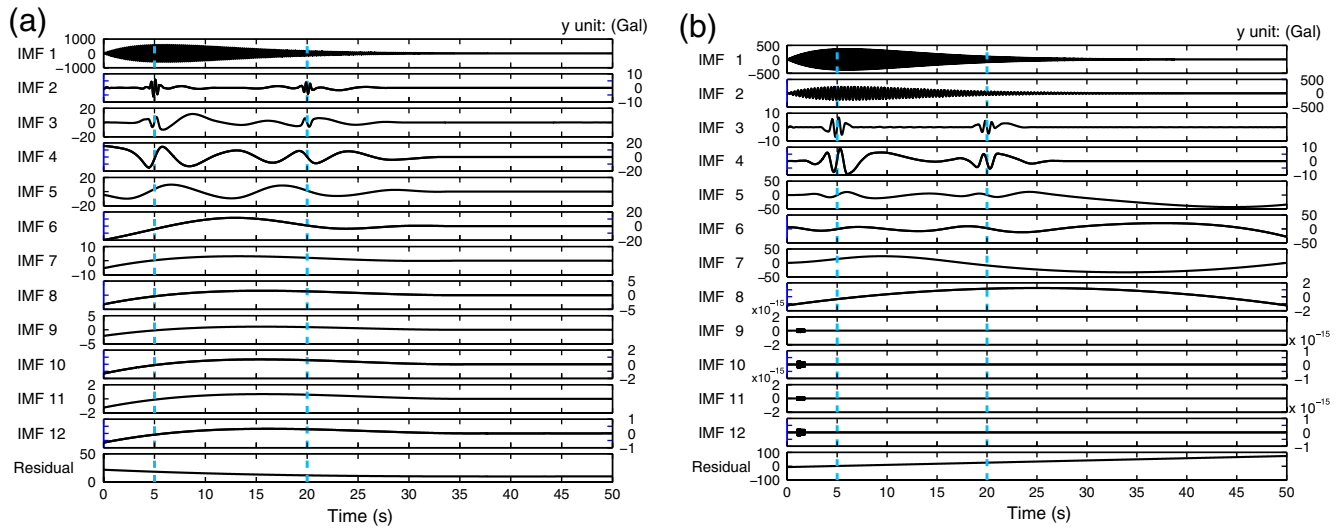


Figure 4. The IMF results of EMD processing of the numerical waveform model. Dashed lines show the time divisions of the given offset models. (a) Model 1, (b) model 2. The color version of this figure is available only in the electronic edition.

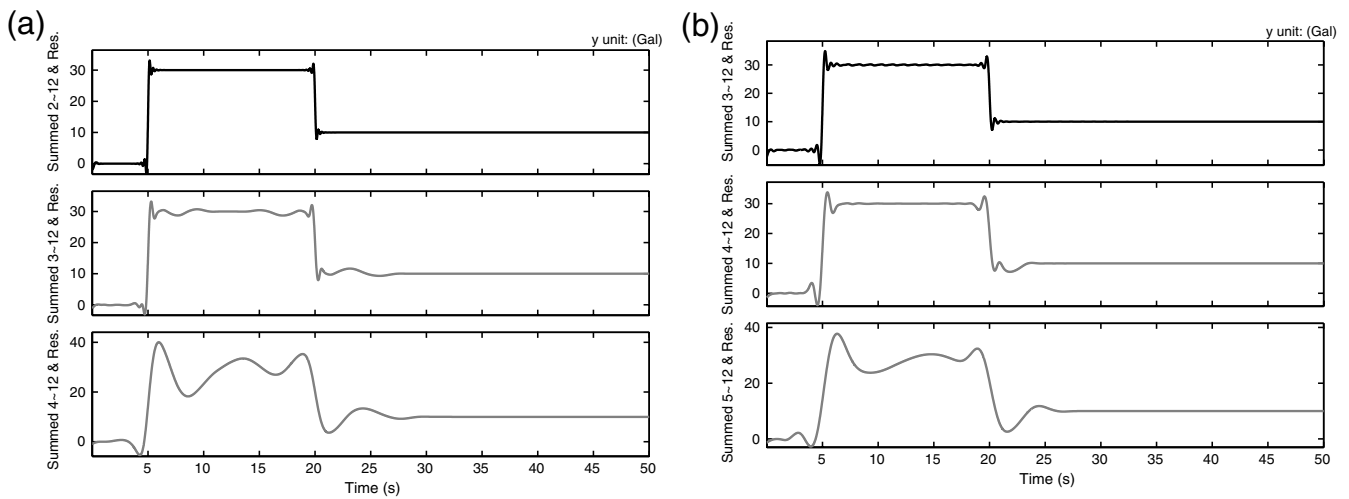


Figure 5. Three of the results that are most similar with the original drift model (black line) and two nearly summed results (gray lines). (a) Numerical waveform model 1, summed from modes 2, 3, 4–12, and residual mode. (b) Numerical waveform model 2, summed from modes 3, 4, 5–12, and residual mode.

$$r_1 - c_2 = r_2; \dots; r_{n-1} - c_n = r_n. \tag{6}$$

Finally, n IMFs are decomposed from these sifting processes. The next question then is the quantity of modes that can be decomposed per signal. Huang *et al.* (1998) mentioned as a cutoff point the residual r_n being so small (a monotonic function) that no further IMF could be decomposed. Flandrin (2004) tried to systematize this procedure by decomposing the signal of white noise. They found that even a complex frequency-content signal such as white noise has mode numbers of less than or equal to an order of two relative to the total number of data points. Wu and Huang (2008) set the effective mode number as approximately an

order of two to the total number of data points minus one, giving total IMF of

$$n = \log_2(p_{\text{total}}), \tag{7}$$

$$n_{\text{IMF}} = \text{ROU}(n) - 1, \tag{8}$$

where p_{total} is total number of data points of original data $X(t)$, n_{IMF} is the total IMF number from the sifting process, and $\text{ROU}(n)$ is the round down for the value of n (i.e., no decimal places).

In this study, the improved EMD process of Wu and Huang (2008) is used to decompose man-made numerical

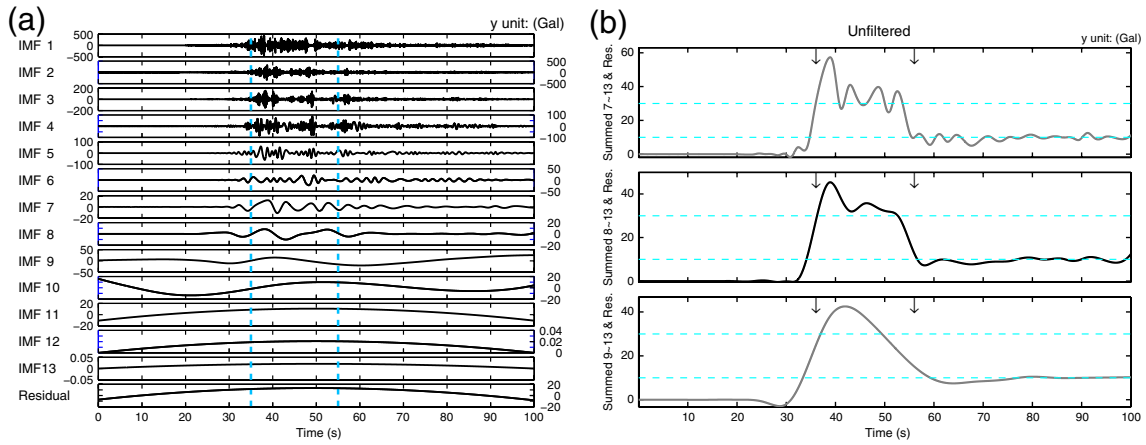


Figure 6. EMD results of numerical waveform model 3 (without any filtering). (a) The IMF results. (b) Three of the results that are most similar to the original drift model (black line) and two nearly summed results (gray lines); down arrows show divided time, and dashed lines show the offset value of design drift model, summed from modes 7, 8, 9–13, and residual mode. The color version of this figure is available only in the electronic edition.

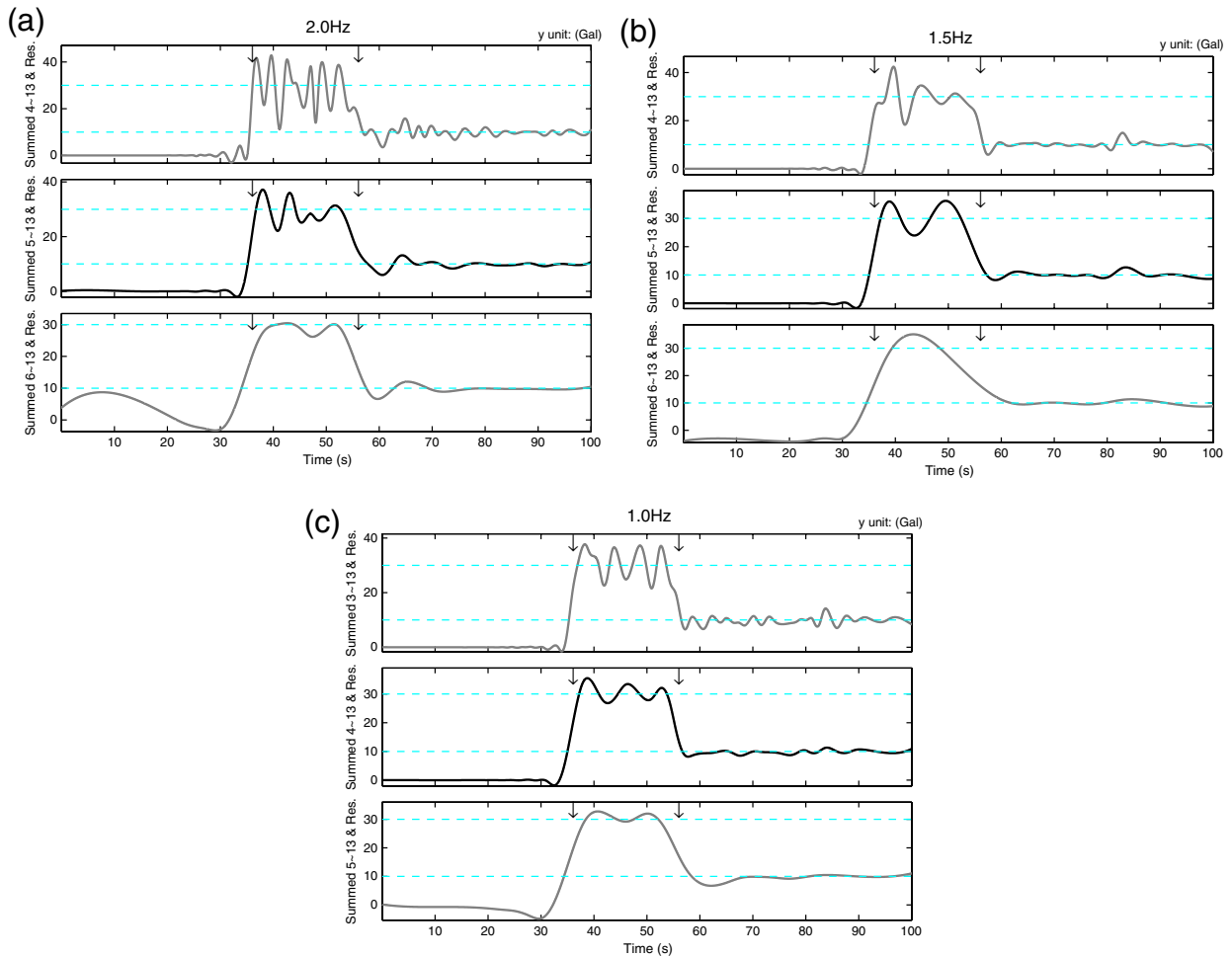


Figure 7. Three of the results for summing the higher modes for numerical waveform model 3 with low-pass filtered after adding the given drift model. Corner frequency of low-pass filtering are (a) 2.0 Hz, (b) 1.5 Hz, and (c) 1.0 Hz. The color version of this figure is available only in the electronic edition.

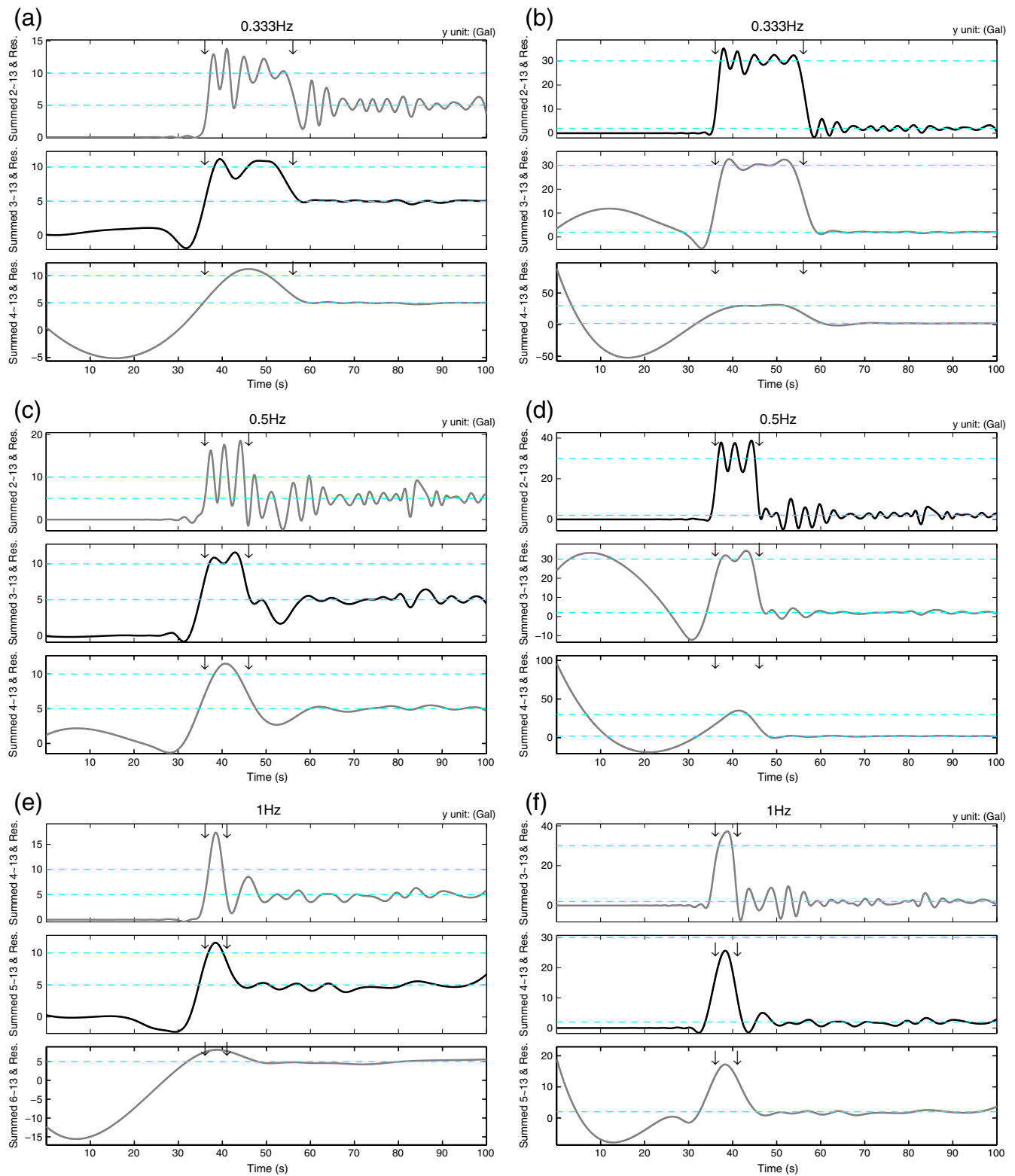


Figure 8. The summed results of low-pass filtering for model 3 with 0.333-Hz corner frequency, 20-s period of design offset (down arrows at 35 and 55 s). Dashed lines indicate amplitude of offset: (a) 10 Gal, 5 Gal and (b) 30 Gal, 2 Gal; (c) 10 Gal, 5 Gal and (d) 30 Gal, 2 Gal have 0.5-Hz corner frequency, 10-s period of design offset (down arrows at 35 and 45 s); (e) 10 Gal, 5 Gal and (f) 30 Gal, 2 Gal have 1-Hz corner frequency, 5-s period of design offset (down arrows at 35 and 40 s). The color version of this figure is available only in the electronic edition.

waveform models and real seismic data to correct the problem of baseline drift.

Numerical Waveform Model

In order to verify the ability of the improved EMD process of Wu and Huang (2008) to deal with baseline drift problems, several numerical waveform models are examined. First, we compose a single- or double-frequency-content sinusoidal wave designed with a wave package that will attenuate with time. Two obvious offsets based on the assumption of the baseline drift model of Iwan *et al.* (1985) are added to these waveforms (Fig. 2). The equation for the single-frequency-content signal is as follows (model 1):

$$y = \frac{600}{0.141} \times \sin(\pi t) \times \exp(-8t) \times \sin(10\pi t), \quad (9)$$

where the unit of y is acceleration ground motion (Gal). The obvious offsets are set at 5 and 20 s (Fig. 2a).

The double-frequency-content signal is shown in Figure 2b. The equation is as follows (model 2):

$$y = \frac{600}{0.294} \times \sin(\pi t) \times \exp(-8t) \times [1.3 \times \sin(20\pi t) + 0.8 \times \sin(6\pi t)]. \quad (10)$$

After considering a simple frequency-content signal, a complex frequency-content signal corresponding to a real world scenario is constructed. The third numerical model is made from real seismic data of the May 2008 Wenchuan, China, earthquake. The seismic data are provided from the Institute of Engineering Mechanics, China Earthquake Administration (see Data and Resources). The acceleration data are high-pass filtered first to eliminate any original possible baseline drift problem before adding the given offsets of this paper's model. The offsets of the drifting model are set at 35 and 55 s (Fig. 3; model 3).

Improved EMD Process and Numerical Waveform Models

Several IMF components, decomposed from the first and second numerical waveform models by EMD, are shown in Figure 4. There are obvious discontinuities for the time divisions of the given drift models for lower IMF components (IMF2 and IMF3). The final offset in residual mode indicated the second offset (10 Gal) of model 1; these offsets occurred at 5 s (30 Gal) and 20 s (10 Gal) (Fig. 4a). Obvious discontinuities also occurred at drift times for lower IMF components (IMF3 and IMF4); however, the final offset is not shown in the residual mode of model 2 (Fig. 4b).

Because of the frequency content becoming lower with increasing IMF numbers (Zhang *et al.*, 2003), the steplike drift model (which can be imaged as a low-frequency signal)

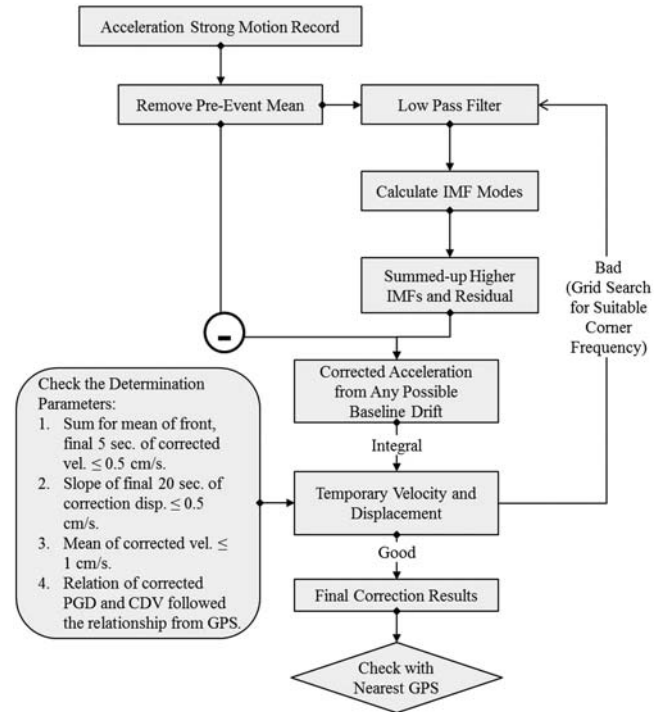


Figure 9. Semiautomatic EMD-derived baseline correction scheme of this study.

should occur at the higher or highest IMF modes. The original drift model did not show in the highest mode or residual mode. The higher modes were summed, and the three results that were most similar to the original drift model are shown in Figure 5. Offset can clearly be identified in shape and value for waveform model 1 (Fig. 5a) from summing modes 2–12 and the residual modes. It is also recognizable from summing results for waveform model 2, but the modes (summing 3–12 and residual modes) were different from the previous example (Fig. 5b).

Figure 6 shows waveform model 3 (without any filtering on raw data). The phenomenon of discontinuity is evident in each of the IMFs of models 1 and 2, but this is not so apparent in model 3, especially in the lower-order IMFs. The trend in the steplike drift model can still be found by summing modes 8–13 and residual modes. Figure 6b shows the results of summing these higher modes.

These results suggest the following assumption: simple or lesser frequency-content signals have a greater decomposed result, and a given drift model can be found by summing higher and residual modes. To test this, Fourier-based low-pass filtering with different corner frequencies was applied to numerical waveform model 3 after summing the drift model to reduce frequency content. Figure 7 shows that the lower frequency content of the original signal does have better decomposed results. At 1 Hz (Fig. 7c), the result shows the closest shape and offset value to the original steplike drift

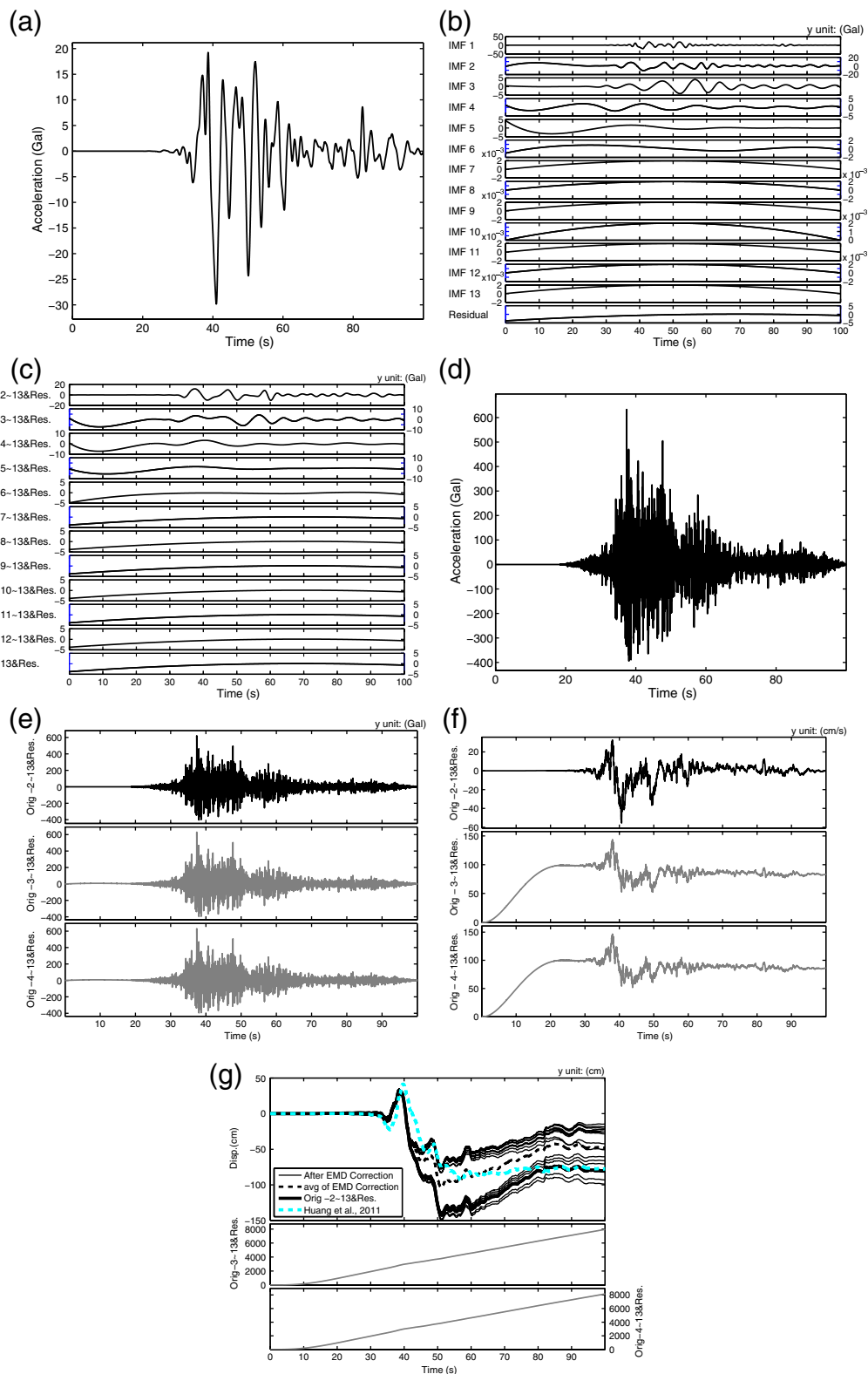


Figure 10. Examples of the EMD-derived baseline correction scheme of this study: (a) acceleration data with low-pass filtering (corner frequency, 0.385 Hz) for station 51SFB in Z component for the May 2008 Wenchuan, China, earthquake; (b) 13 IMFs and residual from EMD process; (c) summed results from modes 2, 3, 4...13 and residual mode; (d) original acceleration data with removed-front 3-s mean; (e) the result of original minus summed IMFs, modes 2, 3, 4...13, and residual mode in acceleration (thick black line, suitable correction results; gray lines, nearby modes); (f) velocity; (g) displacement (light dashed line, correction from [Huang et al. \[2011\]](#); thin black lines, final 15 matches; black dashed line, average of these results). The color version of this figure is available only in the electronic edition.

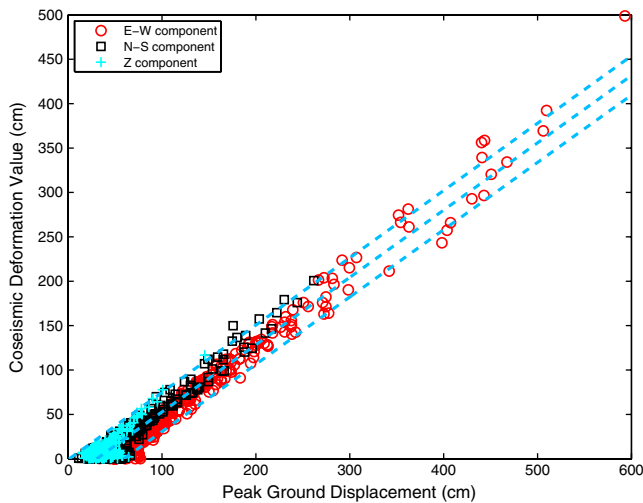


Figure 11. The relationship between PGD and CDV for 1-Hz continued GPS data from the 2011 Tohoku earthquake for east–west, north–south, and vertical components. Dashed lines are the regression lines and the ± 2 standard deviation values for the equation, $CDV = (0.76 \times PGD) - 22.97 \pm 11.04$; 395 stations were used. The color version of this figure is available only in the electronic edition.

model. This result is better than filtering at 1.5 and 2 Hz (Fig. 7a,b) and the unfiltered result (Fig. 6b). Several tests were made and the summing of higher modes treated as a quality index in the next section.

Different Tests for Summing Higher IMFs

Following the above assumption, an induction method is used in this section. Several different tests using different offsets and filtering signals are conducted to find which parameters most influence the results of decomposition. The parameters include the period of given drift models, corner frequencies for low-pass filtering, and the amplitude of given offsets.

Figure 8 shows characteristic differences between the summed results for each parameter; the black lines are the suitable decomposed results. These results fit the original man-made drift models for the different parameters. The findings can be summarized as follows: (1) if a suitable corner frequency for low-pass filtering is implemented first to reduce frequency content, the trend in the given offset model can be more readily found from summing higher IMFs; (2) the suitable corner frequency decreases with increasing period for the given offset; and (3) the suitable corner frequency is also influenced by the amplitude of the given drift models. Additionally, for the results of summing higher IMFs for numerical waveform model 3, although low-pass filtering before EMD processing helped reduce frequency content, some ripples still occurred in the summed waveform. This suggests some limitations, perhaps due to the rectangular shape of the step function in the filter bank for EMD processing. However, the rectangle shape of the step function is a simplistic drift model,

and it should be more complex during strong shaking, which suggests there still exist some opportunities to correct the baseline drift problem through the EMD process. Additionally, the assumption can be modified as if suitable low-pass filtering had already been applied. Good correction results can be achieved regardless of the steplike drift model.

New EMD-Derived Baseline Correction Scheme

As the suitable corner frequency of low-pass filtering is related to the period of drift models and amplitude of drift offsets, the shape of real drift offsets for real seismic data is not clear. There are many uncertainties in applying the improved EMD process to real seismic data as the shape of drift model may not be sharp and rectangular-like in offset. Therefore, the grid-search method is applied to find a suitable corner frequency for low-pass filtering of real seismic data in this study.

The assumed baseline correction scheme is as follows (see flow chart in Fig. 9 and example in Fig. 10): (1) For original acceleration seismic records, the preevent mean is first removed (this is the start of the record plus three seconds before the earthquake signal); additionally, acceleration data is subject to low-pass filtering with the corner frequency (Fig. 10a) changed several times during the grid-search scheme. (2) IMFs are calculated for the filtered signal (Fig. 10b), and summing of the higher modes and residuals is conducted for each mode (2, 3, 4...) to the highest mode (Fig. 10c). (3) As one of the summed results may relate to drift offset in acceleration, it may be eliminated from the difference between raw data and real ground motion; therefore, each summed result is subtracted from unfiltered seismic data with removed-front 3-s mean (Fig. 10d) and then double integrated for velocity and displacement field (Fig. 10e–g). Finally, (4) processes (1)–(3) are repeated continuously until the most suitable corner frequency and its corrected displacement are found. Determination of whether the correction is good or not (i.e., which corner frequency should be applied) is based on the mean of the front and final parts of corrected velocity being near zero, the final portion of the corrected displacement being a flat straight line, the mean of corrected velocity being near zero, and following the relation between corrected peak ground displacement (PGD) and coseismic deformation value (CDV) for the EMD correction results.

After adding the aforementioned parameters to the model, the EMD-derived baseline correction scheme can become a semiautomatic process. As an example, we look at the acceleration record of the Z component at station 51SFB for the May 2008 Wenchuan, China, earthquake. To change corner frequencies for low-pass filtering, we first conduct a grid-search scheme for frequencies 0.1–2.5 Hz. The minus-summed-higher-modes process is considered for each modes (2, 3, 4...) to the highest mode. The total numbers of matches for checking is 19,200 (i.e., a frequency interval of 0.001 Hz and subtraction of each summed mode gives 2400×8). If,

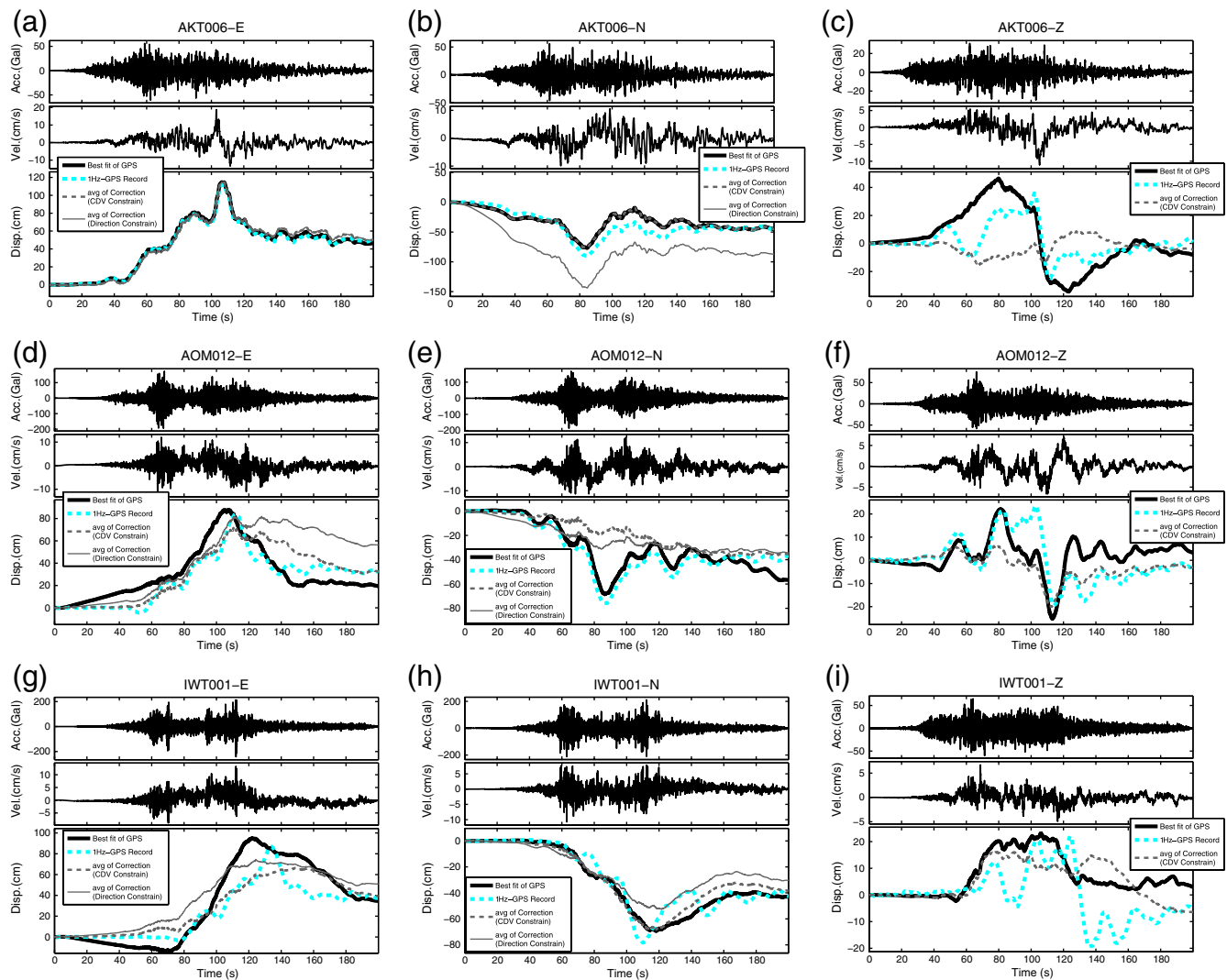


Figure 12. The corrected results from this study for east, north, and vertical components: Station AKT006 (at location A of Fig. 13): (a) E, (b) N, and (c) Z component. Station AOM012 (at location B of Fig. 13): (d) E, (e) N, and (f) Z. Station IWT001 (at location C of Fig. 13): (g) E, (h) N, and (i) Z. Station IWT019 (at location D of Fig. 13): (j) E, (k) N, and (l) Z. Station IWT009 (at location E of Fig. 13): (m) E, (n) N, and (o) Z. Station AKT023 (at location F of Fig. 13): (p) E, (q) N, and (r) Z. The parameters of each station are listed in Table 1. The color version of this figure is available only in the electronic edition. (Continued)

however, the limit for these results is given such that the sum of the average of the front and final 5 s from velocity data is less than or equal to 0.5 cm/s, the matches reduce to 192. Moreover, the matches can be reduced to 114 if the absolute value of slope of displacement for the final 20 s is set to be less than or equal to 0.5 cm/s. The matches can be further reduced to 56 if the mean of absolute value of velocity is set at less than or equal to 1 cm/s. Notably, there are still several anomalous results whereby PGD is large but CDV is relatively small. It is important in this elimination process to establish an acceptable indicator for correlation between these two parameters. Figure 11 plots the correlation between PGD and CDV for the 2011 Tohoku earthquake. Data is based on 1-Hz GPS data collected from the Geospatial Information Authority (GSI) website (see [Data and Resources](#)).

If this correlation is taken as a guide, then a large number of outliers can be removed from our above matches, reducing the number of potential matches to just 15 (Fig. 10g, thin black lines). Using this elimination approach, the most suitable correction-displacement time history can be found if there is some constraint (such as GPS or correction from other baseline correction method) for these final matches.

The most suitable frequency for the example of the Z component at station 51SFB during the May 2008 Wenchuan earthquake is 0.385 Hz. Figure 10 shows the corrected waveforms as black lines in Figure 10e–g. These compare reasonably with the corrected results from the semiautomatic three-part baseline correction method based on the simple assumption from [Wu and Wu \(2007\)](#) found in [Huang et al. \(2011\)](#) (Fig. 10g, light dash line). The CDVs are similar, but

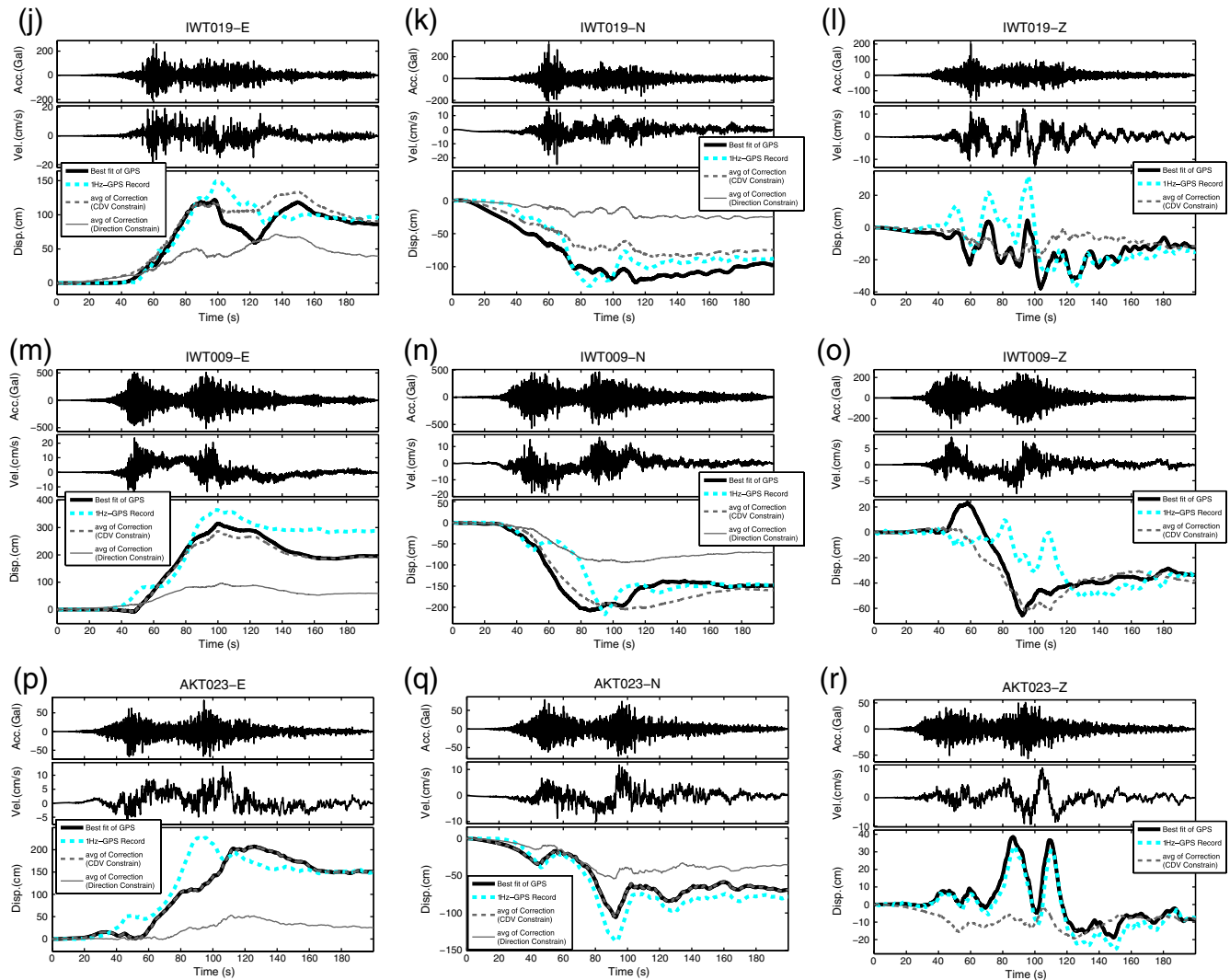


Figure 12. Continued.

PGD values and the record of the shaking history of displacement have some differences.

Corrected-Displacement Time Histories Compared with Nearest GPS Data

The 11 March 2011 Tohoku earthquake is one of the largest earthquakes ever, at M_w 9.0. This event was recorded at 273 K-NET strong-motion stations and 395 1-Hz GPS stations of Japan's GEONET system. Although the epicenter was 150 km off the east coast of Honshu, maximum shaking was $2.7g$. PGA (K-NET MYG004 station) and coseismic deformation was at 5 m (GEONET Osika station 0550) in the Sendai area. For this earthquake, Japan's dense and comprehensive network provides a good opportunity to check corrected-displacement time history using the EMD-derived baseline correction scheme.

Because of the above inconsistencies between our corrected-displacement record and Huang *et al.* (2011) (Fig. 10e–g), as well as a lack of GPS data and shaking processes not being so clear at strong-motion stations in China's Wenchuan region (Working Group of the Crustal Motion Observation Network of China Project, 2008), we choose the 1-Hz continuous GPS records of Japan's GEONET (data source GSI; see Data and Resources) for our comparative study with observed displacement. Moreover, the averages of final correction show a reasonable displacement time history in Wenchuan's case, and we try to add more constraints to deal with different data and make this correction scheme more useful for different regions that lack continuous GPS measurement: (1) Direction of movement can be easily obtained from fault plane solution. (2) CDV measurements can be obtained daily from a GPS station (in this case we consider the CDV of continuous GPS record as the daily solution).

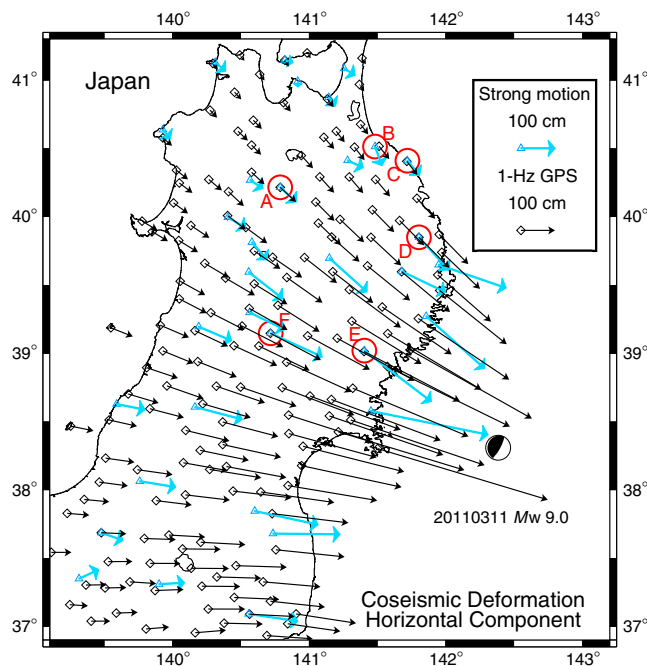


Figure 13. The distribution of stations and CDVs calculated in this study; triangles show K-NET strong-motion stations; diamonds show the GEONET 1-Hz continues GPS stations; circles show the location of example stations that are corrected in this study (see Fig. 12). The color version of this figure is available only in the electronic edition.

Figure 12 shows the correction result of averaging solutions in the same direction as structure movement (thin dash-dotted line), averaging solutions with CDV constraint; the constraint set here is the CDV of each solution $\pm 40\%$ of CDV from GPS measurement, at least searching for the 40-cm range when the CDV from the GPS is smaller than 20 cm (thin dash line), CDV from the nearest GPS measurement, and the most reliable solution (thick solid line) for horizontal components. Because the direction of movement is not easy to obtain in the vertical component, whether it is subsidence or elevated motion for each stations in this case, the averaging solution from direction constraint will not show.

Several strong-motion records from the 2011 Tohoku earthquake are corrected and compared with the results of nearby GPS measurements. The distribution of stations in eastern Japan is shown in Figure 13. Figure 12 shows comparative results for several close station pairs (locations marked in Fig. 13). Although not totally the same, the corrected waveforms of this study have good agreement with the trend of the shaking process, PGD, and CDV (Figs. 12 and 14; Table 1). The regional trend also shows that the corrected CDV of this study fits GPS measurement in direction and value (Fig. 13). Finally, the misfit range is calculated for each correction result using the equation

$$\text{Misfit} = 1 - r(\text{cor}, \text{obs}), \quad (11)$$

where r is the correlation coefficient between the whole record of corrected-displacement time history in this study and

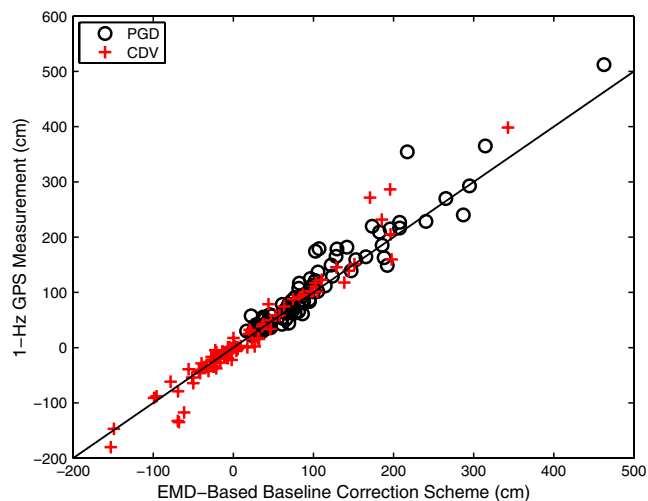


Figure 14. PGD and CDV comparison between the semiautomatic EMD-derived baseline correction scheme of this study for stations marked in triangles on Figure 13 and nearest 1-Hz GPS measurements. The oblique line is the same size ratio. The color version of this figure is available only in the electronic edition.

the observation from the nearest GPS. The average misfit is 0.152; residual in PGD and CDV predictions are 12.3 and 10.3 cm, respectively, of example stations (Fig. 12) for the correction scheme in this study. It shows a good ability for an EMD-derived baseline correction scheme to deal with the drift problem. Otherwise, misfit and residual values for averaging final solutions from direction and daily CDV constraint show that if we did not have 1-Hz continuous GPS measurement, we need at least daily CDV constraint to get the precise time history (Table 2).

Conclusions

An EMD-derived baseline correction scheme is used in this study and verified against real displacement time history using GPS measurements.

For single- and double-frequency-content models 1 and 2, obvious discontinuities are found at drift times for lower IMF components; however, a drift model can be clearly identified from summing higher IMFs and the residuals of simple frequency-content waveform models. On the other hand, because the lesser frequency-content signal has the greater decomposed result, if a suitable corner frequency for low-pass filtering is first implemented to reduce frequency content, the trend in the given drift model is easily found by summing higher IMFs for a complex frequency content model (i.e., numerical waveform model, model 3). The suitable corner frequency is influenced by the shape of the drift model. A grid-search process can be applied to find a suitable corner frequency when the true shape of the drift model for an earthquake is not clear.

Based on the above, a new semiautomatic EMD-derived baseline correction scheme is implemented. The corrected CDV, PGD, and displacement time history from this method

Table 1
GPS Measurements and PGD and CDV Relationship of EMD-Derived Baseline Correction Method in This Study

Strong-Motion Correction in This Study										GPS Observation				
Longitude (°)	Latitude (°)	Component	PGD (cm)*	CDV (cm) [†]	f_0 (Hz) [‡]	Mode [§]	PGD (cm)**	CDV (cm) ^{††}	Distance (m)	Longitude (°)	Latitude (°)	Code	PGD (cm)*	CDV (cm) [†]
140.7873	40.2152	E	114.8	46.7	0.279	7	114.5	44.7	26.9	140.787334	40.215440	KAZUNO	112	49.3
		N	76.8	-42.6	0.035	4	76.8	-32.2					90.6	-43
		Z	46.5	-6.8	0.468	4	15.6	-2.3					35.9	0.9
141.4805	40.5138	E	87.9	20.3	0.405	3	71.6	31.1	2608	141.511282	40.515360	HACHINOHE	84	32.4
		N	68.4	-55.8	0.155	6	37.1	-18.9					75.8	-39.1
		Z	25.2	5.3	0.142	4	20.3	-2.4					23.7	-2.3
141.7191	40.4099	E	94.8	35.9	0.621	4	66.3	29.7	726.6	141.713135	40.405201	TANEICHI	86.9	38.6
		N	69.4	-42.8	0.778	3	68.1	-28.8					78.4	-40
		Z	23.1	3.8	1.444	5	16.1	5					22.1	-5.5
141.8034	39.8491	E	122.1	87	0.985	2	133.8	75.7	39.5	141.803852	39.849177	IWAIZUMI2	149.4	95.7
		N	123.7	-95.8	0.25	3	84.6	-57.1					129.4	-88.1
		Z	37.9	-11.3	0.164	2	20.9	-7.5					36.7	-14.3
141.4031	39.0187	E	314.5	195.7	1.81	4	286.9	148.4	758.2	141.400855	39.012108	IWATEOHHIGASHI	365	286.5
		N	207.5	-149	1.215	6	204.8	-125.7					216.7	-146.9
		Z	65.4	-33.1	1.75	3	62.2	-26.9					51	-33.8
140.717	39.1462	E	207.6	151.2	0.778	5	207.6	105.8	168.1	140.715050	39.146202	HIGASHINARUSE	226.9	151.1
		N	105.7	-69	0.091	4	105.7	-50.1					137	-78.9
		Z	38.6	-8.5	0.102	6	19.2	-8.6					33.1	-7.6

*PGD: peak ground displacement

†CDV: coseismic deformation value

‡ f_0 : corner frequency used for low-pass filtering in this study

§Mode: the mode number from which modes should be subtracted

||Distance: distance between strong-motion station and GPS station

**PGD: peak ground displacement from averaging solution of CDV constraint

††CDV: coseismic deformation value from averaging solution of CDV constraint

****PGD: peak ground displacement from averaging solution of direction constraint

†††CDV: coseismic deformation value from averaging solution of direction constraint

Table 2
Misfit and Residual of EMD-Derived Baseline Correction Method in This Study and GPS Measurement

Code	Component	PGD ratio*	CDV ratio [†]	Best Fit with GPS			CDV Constraint			Direction Constraint		
				Misfit [‡]	PGD_Res (cm) [§]	CDV_Res (cm)	Misfit [‡]	PGD_Res (cm) [§]	CDV_Res (cm)	Misfit [‡]	PGD_Res (cm) [§]	CDV_Res (cm)
AKT006	E	1.03	0.95	0.001	2.7	2.6	0.005	2.5	4.6	0.005	2.5	4.6
	N	0.85	0.99	0.116	13.8	0.4	0.116	13.8	10.7	0.074	53.1	32.8
	Z	1.30	-7.56	0.214	10.6	7.7	1.411	20.3	3.2			
AOM012	E	1.05	0.63	0.160	3.9	12.1	0.067	12.4	1.3	0.118	2.1	10.2
	N	0.90	1.43	0.056	7.4	16.7	0.347	38.7	20.1	0.156	41	16.7
	Z	1.06	-2.30	0.516	1.5	7.6	0.385	3.4	0.1			
IWT001	E	1.09	0.93	0.057	7.9	2.7	0.071	20.6	8.9	0.077	12.7	0.5
	N	0.89	1.07	0.050	9	2.8	0.060	10.3	11.3	0.078	25.7	16.8
	Z	1.05	-0.69	0.471	1	9.3	0.777	6	10.4			
IWT019	E	0.82	0.91	0.071	27.3	8.8	0.056	15.6	20.1	0.147	77.9	59.7
	N	0.96	1.09	0.047	5.7	7.7	0.058	44.8	31.1	0.159	101.1	71.8
	Z	1.03	0.79	0.291	1.1	3	0.930	15.9	6.8			
IWT009	E	0.86	0.68	0.040	50.5	90.7	0.032	78.2	138	0.083	269.2	234.8
	N	0.96	1.01	0.141	9.2	2.1	0.064	11.9	21.2	0.069	122.5	89.5
	Z	1.28	0.98	0.343	14.4	0.7	0.434	11.3	6.9			
AKT023	E	0.91	1.00	0.115	19.3	0.1	0.115	19.3	45.3	0.144	173.7	130.2
	N	0.77	0.87	0.011	31.3	9.9	0.011	31.3	28.8	0.058	82.9	49.4
	Z	1.17	1.12	0.034	5.4	0.9	0.752	13.9	0.9			
Average				0.152	12.3	10.3	0.316	20.6	20.5	0.097	80.4	59.8

*PGD ratio, PGD from strong-motion correction divided by PGD obtained with GPS.

[†]CDV ratio, CDV from strong-motion correction divided by CDV obtained with GPS.

[‡]Misfit of whole record between correction and GPS observation. Minimum 0 means totally the same phase, maximum 2 means totally opposite phase.

[§]PGD_Res, absolute value of PGD from strong-motion correction minus PGD obtained with GPS.

^{||}CDV_Res, absolute value of CDV from strong-motion correction minus CDV obtained with GPS.

have good agreement with 1-Hz continuous GPS measurement for the 2011 Tohoku earthquake. The average misfit for 33 stations (distribution shown in Fig. 13) is 0.239; residual in PGD and CDV predictions are 17.4 and 14.0 cm, respectively, for the correction scheme in this study.

Data and Resources

This study uses strong-motion data for (1) the May 2008 Wenchuan, China, earthquake, provided by China Strong Motion Networks Center, Institute of Engineering Mechanics, China Earthquake Administration and (2) the 2011 Tohoku earthquake, collected from K-NET, Japan (data are available at <http://www.k-net.bosai.go.jp/>, last accessed September 2012). The 1-Hz continuous GPS records were processed from GSI (Geospatial Information Authority, Japan), NGDS (Nippon GPS Data Service, Japan), Hitz (Hitachi Zosen Co., Japan), GPSS (GPS Solutions, Boulder, Colorado), and VERIPOS (company of instrument and software, United Kingdom). Data can be obtained from the website of GSI at http://rtgps.com/rtnet_dl_eq.php (last accessed September 2012).

Acknowledgments

This study was supported by the National Science Council under Grant Numbers NSC 99-2116-M-008-023 and NSC 100-2116-M-008-013. We appreciate C. M. Lin and C. H. Kuo and S. C. Chang for all the discussions and ideas relating to this topic. Special thanks for Joe Fletcher, two anonymous

reviewers, and our editor for providing lots of excellent comments which helped us in improving this article.

References

- Boore, D. M. (2001). Effect of baseline corrections on displacements and response spectra for several recordings of the 1999 Chi-Chi, Taiwan, earthquake, *Bull. Seismol. Soc. Am.* **91**, no. 5, 1199–1211.
- Boore, D. M. (2003). Analog-to-digital conversion as a source of drifts in displacements derived from digital recordings of ground acceleration, *Bull. Seismol. Soc. Am.* **93**, no. 5, 2017–2024.
- Boore, D. M., and J. J. Bommer (2005). Processing of strong-motion accelerograms: Needs, options and consequences, *Soil Dynam. Earthq. Eng.* **25**, 93–115.
- Boore, D. M., C. D. Stephens, and W. B. Joyner (2002). Comments on baseline correction of digital strong-motion data: Examples from the 1999 Hector Mine, California, earthquake, *Bull. Seismol. Soc. Am.* **92**, no. 4, 1543–1560.
- Chanerley, A. A., and N. A. Alexander (2010). Obtaining estimates of the low-frequency ‘fling’ instrument tilts and displacement time series using wavelet decomposition, *Bull. Earthq. Eng.* **8**, 231–255.
- Chao, W. A., Y. M. Wu, and L. Zhao (2010). An automatic scheme for baseline correction of strong-motion records in coseismic deformation determination, *J. Seismol.* **14**, 495–504.
- Chen, S. M., and C. H. Loh (2007). Estimating permanent ground displacement from near-fault strong-motion accelerograms, *Bull. Seismol. Soc. Am.* **97**, no. 1B, 63–75.
- Flandrin, P., G. Rilling, and P. Gonçalvès (2004). Empirical mode decomposition as a filter bank, *IEEE Signal Process. Lett.* **11**, no. 2, 112–114.
- Graizer, V. (1979). Determination of the true ground displacement by using strong motion records, *Izvestiya Phys. Solid Earth* **15**, 875–885.
- Graizer, V. (2005). Effect of tilt on strong motion data processing, *Soil Dynam. Earthq. Eng.* **25**, 197–204.

- Graizer, V. (2006). Tilts in strong ground motion, *Bull. Seismol. Soc. Am.* **96**, no. 6, 2090–2102.
- Huang, N. E., C. C. Chern, K. Huang, L. W. Salvino, S. R. Long, and K. L. Fan (2001). A new spectral representation of earthquake data: Hilbert spectral analysis of station TCU129, Chi-Chi, Taiwan, 21 September 1999, *Bull. Seismol. Soc. Am.* **91**, no. 5, 1310–1338.
- Huang, J. Y., K. L. Wen, C. T. Chen, and S. C. Su (2011). Coseismic deformation of the 2008 Wenchuan, China earthquake calculated from strong motion data, in *8CUEE Conference Proceedings*, Tokyo, Japan, 7–8 March, Vol. 1, 237–241.
- Huang, N. E., S. Zheng, S. R. Long, M. C. Wu, H. H. Shih, Q. Zheng, N. C. Yen, C. C. Tung, and H. H. Liu (1998). The empirical mode decomposition and Hilbert spectrum for nonlinear and nonstationary time series analysis, *Proc. Roy. Soc. Lond. Math. Phys. Sci.* **454**, 903–995.
- Iwan, W. D., M. A. Moser, and C. Y. Peng (1985). Some observations on strong-motion earthquake measurement using a digital accelerograph, *Bull. Seismol. Soc. Am.* **75**, no. 5, 1225–1246.
- Mallat, S. G. (1989). Theory for multi-resolution signal decomposition: The wavelet representation, *IEEE Trans. Pattern Anal. Mach. Intell.* **11**, no. 7, 674–693.
- Wang, G. Q., D. M. Boore, H. Igel, and X. Y. Zhou (2003). Some observations on collocated and closely spaced strong ground-motion records of the 1999 Chi-Chi, Taiwan, earthquake, *Bull. Seismol. Soc. Am.* **93**, no. 2, 674–693.
- Wang, R. J., B. Schurr, C. Milkereit, Z. G. Shao, and M. P. Jin (2011). An improved automatic scheme for empirical baseline correction of digital strong-motion records, *Bull. Seismol. Soc. Am.* **101**, no. 5, 2029–2044.
- Working Group of the Crustal Motion Observation Network of China Project (2008). Coseismic displacement field of the 2008 M_S 8.0 Wenchuan earthquake determined by GPS, *Sci. China Earth Sci.* **38**, no. 10, 1195–1206 (in Chinese).
- Wu, Y. M., and C. F. Wu (2007). Approximate recovery of coseismic deformation from Taiwan strong-motion records, *J. Seismol.* **11**, 159–170.
- Wu, Z., and N. E. Huang (2008). Ensemble empirical mode decomposition: A noise assisted data analysis method, *Adv. Adapt. Data Anal.* **1**, no. 1, 1–41.
- Zhang, R. R., S. Ma, E. Safak, and S. Hartzell (2003). Hilbert-Huang transform analysis of dynamic and earthquake motion recordings, *J. Eng. Mech.* **129**, no. 8, 861–875.

Department of Earth Sciences
National Central University
Taoyuan 32001, Taiwan (R.O.C.)
jyhuang428@gmail.com
wenkl@earth.ncu.edu.tw
pokayoke69@gmail.com
scsu0514@scman.cwb.gov.tw
(J.-Y.H., K.-L.W., C.-T.C., S.-C.S.)

Institute of Geophysics
China Earthquake Administration
Beijing 100081, China
beerli@vip.sina.com
xiejunjv05@mails.ucas.ac.cn
(X.-J.L., J.-J.X.)

Manuscript received 13 September 2012